INTERACTIVE CONTROL OF MICRO-MIXING AND IN-SITU GELATION OF HYDROGELS FOR CELL-LADEN CYLINDRICAL MICROGEL FABRICATION

J. OH[a†], S. C. CHOI[b†], D. LEE[c,d†], K. I. KANG[e], J. JUNG[a*]

[a]*Department of Nano-Bio Mechanical System Engineering, Chonbuk National University, Jeonju 561-756, South Korea*
[b]*Thermochemical Energy System R&BD Group, Korea Institute of Industrial Technology, Cheonan, Korea*
[c]*Division of Mechanical Design Engineering, Chonbuk National University, Jeonju 561-756, South Korea*
[b]*Hemorheology Research Institute, Chonbuk National University, Jeonju 561-756, South Korea*
[e]*Department of Bio-Nano System Engineering, Chonbuk National University, Jeonju 561-756, South Korea*

In this paper, we present a system for an interactive control of micro-mixing and in-situ gelation of hydrogels. The performance and stability of micro-mixing in the system were simulated using the computer-aided finite element analysis. The fabricated system was tested to confirm the effectiveness of micro-mixing using Rhodamine B solution (RB), brilliant blue solution (BB), and deionized water (DW). The experimental results demonstrated that the system can effectively perform the micro-mixing of RB and BB solutions by changing the DW flow rates. The interactive control of micro-mixing and in-situ gelation of N-carboxyethyl chitosan (NCC) and gelatin by oxidized dextran (ODX) was experimentally confirmed, resulting in a successful fabrication of in-situ gelable cell-free and cell-laden cylindrical microgels of a variety of lengths. The biocompatibility and non-cytotoxicity were demonstrated using human umbilical vein endothelial cells (HUVECs), showing a high cell viability. Therefore, the suggested system can serve as a highly effective tool for the fabrication of in-situ gelable cell-free or cell-laden cylindrical microgels in biomedical research.

1. Introduction

In the field of biomedical engineering, the importance of rapid and effective mixing of polymers composed of a variety of molecules (biological or otherwise) cannot be overestimated. The rapid evolution of microfluidic technologies has played an important role in the potential applications of micro-mixing in biomedical engineering. Therefore, microfluidics-assisted micro-mixing technologies have been developed for a wide range of biomedical applications, including drug screening [1-3], enzyme assay [4-6], and DNA analysis [7-9].

For instance, Burke and Regnier developed a passive, stopped-flow micro-mixer for kinetic enzyme assays [10]. Furthermore, Park *et al.* used a passive three-dimensional (3D) serpentine micro-mixer to perform kinetic enzyme assays for biological screening [11]. Likewise, Tseng *et al.* verified the capabilities of the active surface-acoustic wave micro-mixer for enzyme assays [12] and Apetri *et al.* performed protein folding using passive, continuous-flow capillary mixing[13]. Furthermore, Chang *et al.* mixed two droplets with PCR reagents and cDNA samples

---

using an active electrowetting-on-dielectric effect mixer for bio-analytical processes [14]. Finally, Hashimoto *et al.* applied a passive Y-shape mixer to serial processing of biological reactions using flow-through microfluidic devices for bio-analytical processes[15].

In this study, we present the cell-laden cylindrical microgel fabrication method which simultaneously facilitates micro-mixing and in-situ crosslinking of chitosan and gelatin cell-laden hydrogels. The method uses a glass capillary-based cross-shape passive micro-mixer using dual molecular transport. The dual-diffusion function of our micro-mixer allows for controlling the micro-mixing rate and in-situ crosslinking rate of two different hydrogels changing the flow rate. The flow of dextran-based cross-linker located in the center of glass capillary enables in-situ cross-linking of two hydrogels.

2. Experimental

2.1 Hydrogel preparation

Cell-embedded cylindrical microgels were fabricated using in-situ gelablebiomaterials, N-carboxyethyl chitosan (NCC), gelatin, and oxidized dextran (ODX) as a cross-linker. The in-situ cross-linking process was initiated between the synthesized NCC (amine groups) mixed with gelatin and ODX (aldehyde groups) via imine formation. Water-soluble NCC, gelatin, and ODX were prepared as follows: 400 ml deionized water (DW) containing 5.6 ml acrylic acid was prepared. 800mg chitosan (Sigma-Aldrich, MO, USA) were mixed with 400 ml DW. The solution was gently stirred for 48 hours (400 rpm, 50 °C). Then, the chitosan solution was converted into its sodium salt by adding 0.1 M NaOH. 8mg gelatin (Sigma-Aldrich, MO, USA) was dissolved in 200 ml DW.

ODX was served as a cross-linker for the NCC solution by introducing aldehyde functionalities. To prepare ODX, 624 g $NaIO_4$ solution (dissolved in 80 ml DW) and 320 ml dextran solution (1.25 w/v) (Sigma-Aldrich, MO, USA) were mixed. The mixed dextran solution was stirred for 48 hours (400 rpm, room temperature). The unreacted $NaIO_4$ was quenched by adding 2.45 g polyethylene glycol (Sigma-Aldrich, MO, USA) during stirring. Both the gelatin and dextran mixtures were then dialyzed (MWCO 12000) for 72 hours and pure water soluble NCC and ODX were lyophilized for the experiments.

2.2 Finite element analysis for design optimization

The parameters related to the performance of the micro-mixer were studied using finite element analysis software (Comsol Multiphysics, Comsol Inc., MA, USA) prior to fabrication. A 3D, glass, capillary-based geometry of the micro-mixer was modeled to generate co-axial flow (see Figure 1). The finite-element microfluidic model was composed of three inlets, one each for the RB solution, the BB solution, and D Wusing a glass capillary (ID = 580 μm). DW was introduced into the core region, while the two solutions (RB and BB) were infused into the shell region.
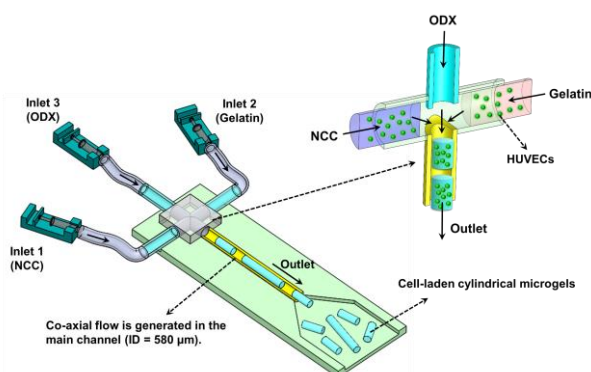

Fig. 1. Schematic representation of the in-situ gelable cylindrical micorgel fabrication system using NCC, gelatin, and ODX (cross-linker). NCC = N-carboxyethyl chitosan; ODX = oxidized dextran; HUVECs =human umbilical vein endothelial cells.

Micro-mixing was simulated using a mathematical coupling technique between two physics models: the laminar flow model and the molecular transport model. For the laminar flow model, the continuity and Navier-Stokes equations were applied to describe conservation of mass and momentum, respectively, as shown in Eqs. (1)-(2). We assumed incompressible steady-state co-axial flow at room temperature. For the molecular transport model, the chemical mass balance equation was used to consider passive molecular interactions between the diluted molecules (RB and BB) and DW (see Eq. (3)).

$$\nabla \cdot (\rho \mathbf{u}) = 0 \qquad (1)$$

$$\rho \frac{\partial \mathbf{u}}{\partial t} + \mathbf{u} \cdot \nabla \mathbf{u} = -\nabla p + \mu \nabla^2 \mathbf{u} + \mathbf{F} \qquad (2)$$

$$\frac{\partial c}{\partial t} + \mathbf{u} \cdot \nabla c = \nabla \cdot (D \nabla c) + R \qquad (3)$$

Where u is the velocity vector (m/s), ρ is the density (kg/m^3), p is the pressure (Pa), F is the volume force vector (N/m^3), μ is the dynamic viscosity (Pa·s), c is the concentration of the RB and BB solutions (mol/m^3), D is the diffusion coefficient (m^2/s), and R is the reaction rate [mol/(m^3·s)]. Boundary conditions for the RB and BB solutions were applied with the same flow rates (2,000μl/h) at the inlets, while the infused flow rate of DW at the inlet varied from 3,000 to 5,000 μl/h. Viscosities of the RB and BB solutions were assumed to be equivalent to that of DW. The outlet of the mixer was at zero pressure and no slip occurred at the wall. The initial concentration of the RB and BB solutions at the inlets was 2.0 mol/m^3 and DW was introduced at the concentration of 0 mol/m^3. The diffusion coefficient of the RB solution in DW was 3.6×10^{-10} m^2/s, while that of the BB solution was 2.8×10^{-9} m^2/s. The walls of the microfluidic channels were assumed to be completely insulated and convective flux was permitted at the outlet.

The micro-mixer model was optimally meshed to solve the finite-element-based multiphysics equations at the stationary condition. The results were analyzed to investigate the performance and stability of the micro-mixer. Critical data were post-processed for the purposes of visualization.

2.3 Cross-shape passive micro-mixer fabrication

The cross-shape passive micro-mixer was fabricated using the design suggested by the computer-aided simulation. The micro-mixer device consisted of three inlets, one junction, and one outlet (see Figure 1). Three-dimensional microfluidic channels for inlets and an outlet were prepared using four 580-μm-ID glass capillaries (World Precision Instruments, Inc., FL, USA). The junctions of the three inlets were connected and insulated with a PDMS block (10 mm x 10 mm x 5 mm). Figure 1 shows the internal geometry of the micro-mixer at the junction. The inlet 3 was aligned towards the outlet to generate 3D co-axial flow. Inlets 2 and 3 were located perpendicular to the outlet. All components (four glass capillaries and one PDMS block) were permanently fixed on a slide glass (25 mm × 75 mm). Three fluids were then transferred into three different glass syringes (5 mL) and placed in syringe pumps (Genie Touch, Kent Scientific, Inc., CT, USA) in order to infuse the fluids into the micro-mixer at a constant rate.

2.4 Experimental performance analysis

Prior to the in-situ microgel fabrication, the performance and stability of a cross-shape passive micro-mixer were investigated using two different fluorescent dyes. In order to visualize molecular transport caused by momentum diffusion, two different dye solutions were prepared using Rhodamine B (MW = 479.01 g/mol; Sigma Aldrich, MO, USA) and Brilliant Blue G-250 (MW = 854.02 g/mol; Sigma Aldrich, MO, USA), both in the concentration of 2.0 mol/m^3. The concentration of the Rhodamine B (RB) solution was set to 2.0 mol/m^3 by mixing 20.0 mg of RB with 20 ml of DW, while that of the Brilliant Blue G-250 (BB) solution was prepared by dissolving 34.2 mg of BB into 20 ml DW. The two solutions were filtered prior to use in order to eliminate undissolved particles.

The fabricated micro-mixerwas experimentally assessed using various DW flow rates. The perfusion rate of DW at inlet 3 varied from 3,000 to 5,000 µl/h. The RB and BB solutions were constantly infused at the flow rate of 2,000 µl/h into inlets 2 and 3, respectively. Temperature variation affecting molecular diffusion was negated by maintaining the experimental environment at room temperature (21 ± 1.0 °C).Passive molecular transport was observed using an optical microscope (Olympus, Tokyo, Japan). Molecular transport was investigated at the distance of 1, 2, 3, 4, 5, and 6 cm from the junction in the direction of the flow.

2.5 Cell preparation

Human umbilical vein endothelial cells (HUVECs) were used to demonstrate the cell viability of the cell-embedded cylindrical microgel. The HUVECs were cultured in M199 containing 1% penicillin-streptomycin, 2 mM L-glutamine, 20% (v/v) fetal bovine serum, and 200 µg/ml endothelial cell growth supplement (all from Invitrogen, Carlsbad, CA, USA). The cells were incubated at 37 °C with 5% CO_2 and the media were refreshed every 3 days.

2.6 Fabrication of cell-laden cylindrical microgel

Prior to infusion, HUVECs were mixed with the NCC and gelatin pre-polymer solutions. The NCC and gelatin pre-polymer solutions with HUVECs were introduced into the micro-mixer through inlets 1 and 2, respectively, at the fixed flow rate of 2,000 µl/h. In addition, ODX was infused into the mixer through inlet 3 at the fixed flow rate of 3,000µl/h. In order to generate cylindrical microgelsof a variety of lengths, the flow rate of ODX was stopped and restarted repeatedly.

The cell viability of the HUVECs embedded in the cylindrical microgel was investigated at day 1 using the live⁄dead cytotoxicity test kits (Invitrogen, Carlsbad, CA, USA). The fluorescent markers in the live/dead assay was diluted in phosphate buffered saline (PBS) to achieve the concentrations of 0.5 µL/mL calcein-AM (green) and 2 µL/mL ethidium homodimer-1 (red), respectively. The cell-embedded microgels in the assay were then incubated at 37 °C for 15 minutes. After rinsing the remained dyes using PBS, the live/dead HUVECs were observed under a fluorescent microscope.

3. Results and Discussion

A computer-aided finite element simulation was performed to optimize the design of a passive micro-mixer.In the simulation, the RB solution, the BB solution, and DW were injected through inlets 1, 2, and 3, respectively, to generate dual molecular transport. As shown in Figure 2, the simulated micro-mixer model was expected to generate stable, co-axial flow depending on the flow rates of DW. The RB and BB solutions were located in the shell region and, congruently with the expectation, DW flowed in the core region. According to the flow rates of the core region(DW), molecules in the RB and BB solutions with the2.0 mol/m³ molecular concentration were transported to DW (0 mol/m³ molecular concentration) via diffusion. All streams maintained stable laminar flows.

Figures 2(a)-(c) illustrate the cross-sectional concentration profiles of the RB and BB solutions at the DW flow rates of 3,000, 4,000, and 5,000 µl/h, respectively, while those of RB and BB were fixed to 2,000 µl/h. In Figure 2(a), when the co-axial flow rate (DW) was 3,000µl/h, dual molecular transport was reduced to minimum. This phenomenon could be the result of the following: 1) the contact area reduction between DW and the RB/BB solutions; 2) decrease in the DW flow velocity, resulting in a decrease of momentum diffusion. In Figure 2(b), as the co-axial flow rate of DW increased to 4,000µl/h, momentum diffusion increased (as compared to momentum diffusion at the flow rate of 3,000µl/h). The elevated DW flow rate produced a greater pressure gradient in the core region, leading to enhanced molecular diffusion. As shown in Figure 2(c), With an increase in the DW flow rate, momentum diffusion further increased up to 5,000 µl/h (see Figure 2(c)).Dual-momentum diffusion of the RB and BB solutions was proportional to the controlled DW flow rate. Based on the simulated results, control of molecular transport could be achieved by changing the co-axial flow rates.
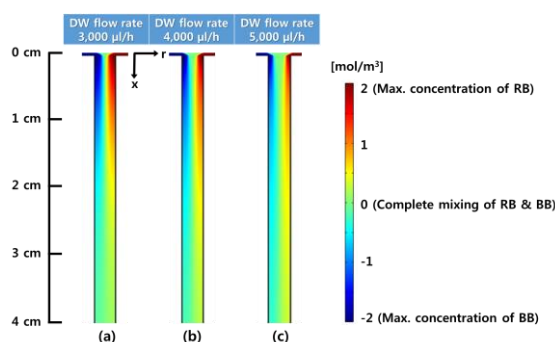
Fig. 2.Cross-sectional concentration profiles of Rhodamine B (RB; 2.0 mol/m³) and Brilliant blue G-250 (BB; 2.0 mol/m³) according to the deionized water (DW) flowrate ((a) 3,000 μl/h; (b) 4,000 μl/h; and (c) 5,000 μl/h). In the scale bar ranging from -2 to 2 mol/m³, 2 mol/m³ was defined as the maximum concentration of RB, while -2 mol/m³indicates the maximum concentration of BB.

To investigate the concentration distribution of the RB and BB solutions due to momentum diffusion, the outlet of the simulated micro-mixer was cross-sectioned in the longitudinal flow direction, 0, 1, 2, 3, 4, 5, and 6 cm from the inlet junction (see Figure 3). Overall, with the increase of the DW flow rate, the momentum diffusion curves of the RB and BB solutions resulted in a steeper increase, indicating a faster molecular diffusion. As the co-axial flow (DW) was developed in the direction of the flow, concentration profiles were uniformly distributed. In Figure 3(c), at the DW flow rate of 5,000 μl/h, the uniform concentration distribution progressed most rapidly, because the elevated pressure gradient (due to a higher DW flow rate) generated a faster molecular transport from the RB/BB solutions to DW.
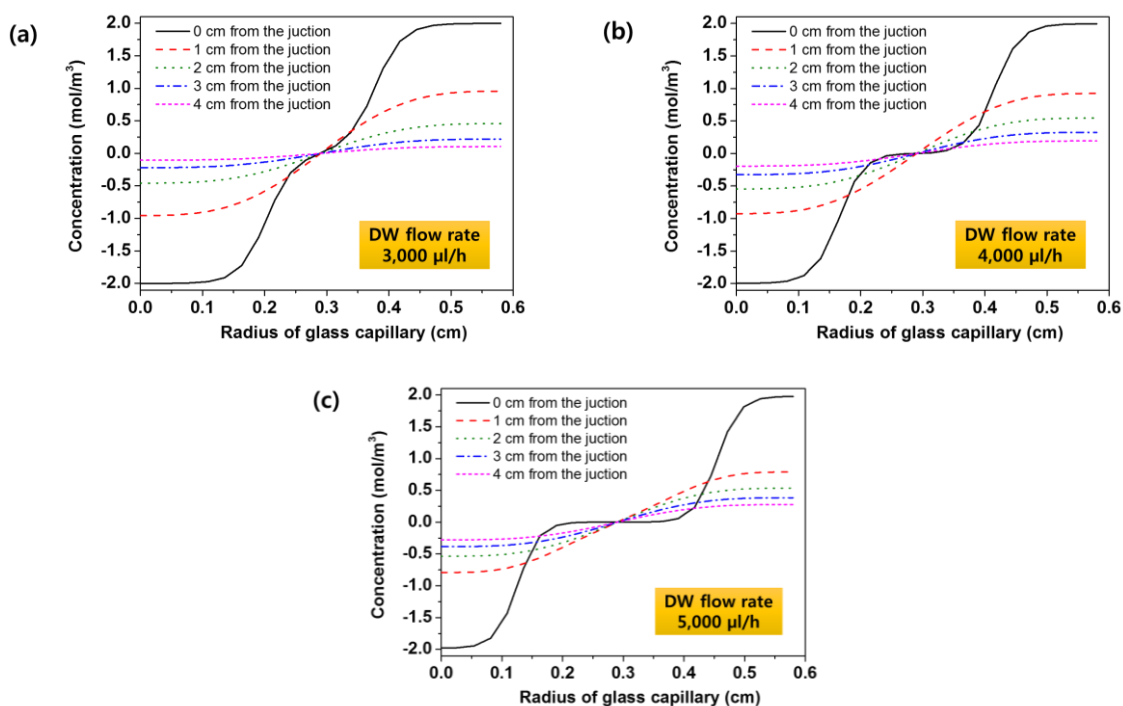

Fig. 3. Cross-sectional concentration distribution of Rhodamine B (RB; 2.0 mol/m3) and Brilliant blue G-250 (BB; 2.0 mol/m³)in the direction of flow at 0, 1, 2, 3, and 4 cm from the junction at the deionized water (DW) flow rates of (a) 3,000 μl/h; (b) 4,000 μl/h; and (c) 5,000 μl/h, respectively. The y-axis was plotted ranging from -2 to 2 mol/m³ (2 mol/m³ = maximum concentration of RB, -2 mol/m³ = maximum concentration of BB).

The designed passive, cross-shape micro-mixer was fabricated and its performance and stability were experimentally examined. Figure 4 shows the microscopic images of surface color changes in molecular concentration according to different DW flow rates. The flow rates of the RB and BB solutions were fixed at 2,000 μl/h. As the RB and BB solutions were introduced into inlets 1 and 2, respectively, it was possible to locate them in the shell region of the co-axial flow. As the flow rate of DW in the core region increased from 3,000 to 5,000 μl/h at inlet 3, an improvement of molecular transport was visually observed, as predicted by the simulated results. At the distance of 1 cm from the junction, the boundary of color mixing between the RB and BB solutions was the highest at the DW flow rate of 5,000 μl/h, representing an enhanced momentum diffusion at a higher DW flow rate. As molecular transport was developed in the flow direction, the apparent boundary color of the RB and BB solutions faded out, indicating progressive micro-mixing. Notably, fast color mixing was observed with the increased DW flow rate due to a greater momentum diffusion, a finding that is compatible with the simulated results. These results indicated that dual molecular transport is proportional to the co-axial flow rate, which could control momentum diffusion.
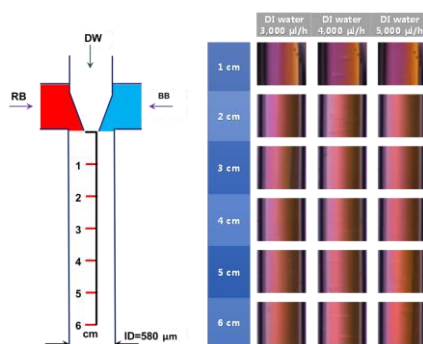

Fig. 4. Microscopic images of the surface color change according to the molecular transport of the Rhodamine B (RB) and Brilliant Blue G-250 (BB) solutions controlled by the deionized water (DW) flow rate as a function of longitudinal distance (1, 2, 3, 4, 5, and 6 cm) from the junction.

Using the prepared passive micro-mixing system, the NCC, gelatin, and ODX pre-polymer solutions were infused through inlets 1, 2, and 3, respectively; then, they were uniformly mixed. It was observed that ODX helped in gelating NCC and gelatin, generating in-situ gelable cylindrical microgels. Figure 5(a) shows a microscopic image of the generated cell-free cylindrical microgels. As the flow rate of ODX was repeatedly stopped and restarted at different time intervals, the cylindrical microgels were successfully fabricated in a variety of lengths. The flow rates of ODX pre-polymer solution, located in the core region, could interactively control the mixing and cross-linking ratios between ODX and two hydrogels (NCC and gelatin in the shell region), resulting in a controlled fabrication of in-situ gelable cylindrical microgels.
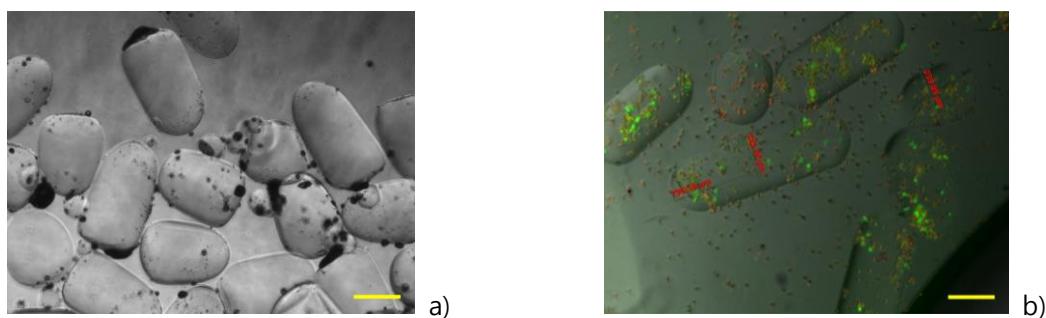

Fig. 5. (a) Microscopic image of cell-free cylindrical microgels and (b) fluorescent microscopic image of cell-embedded cylindrical microgels (green indicates live cells; red indicates dead cells). Scale bar = 200 μm.

The cell viability of the HUVECs embedded in the in-situ gelable cylindrical microgels was investigated. Figure 5(b) shows a fluorescent microscopic image of cell-embedded cylindrical microgels at day 1. It was observed that the micro-mixing in the system contributed to the even distribution of HUVECs inside the cylindrical microgels. Almost all embedded-HUVECs were found alive, indicated with green, while several dead cells stained with red were observed. As a result, cell viability at day 1 was estimated to be around 86 ± 4 %. These results confirm that the in-situ gelation method to fabricate cell-laden cylindrical micogels is biocompatible andnon-cytotoxic.

In conclusion, micro-mixing and in-situ gelation of hydrogels in the system were very effectively and interactively controlled. Therefore, the in-situ gelable fabrication system for cell-laden cylindrical microgels in a variety of lengths can be meaningfully used as an alternative tool in a wide range of tissue and biomedical engineering applications.

4. Conclusion

The simulation performed prior to the device fabrication predicted that micro-mixing using the RB and BB solutions in the system could be interactively controlled by changing the DW flow rates in the core region. Based on the simulated results, the microfluidic system was successfully fabricated and tested to generate in-situ gelable cylindrical microgels. Both cell-free and cell-laden cylindrical microgels using NCC and gelatin hydrogels were fabricated by controlling the ODX (cross-linker) flow rates. The viability of HUVECs embedded in the cylindrical microgels was very high, demonstrating their biocompatibility and non-cytotoxicity. Therefore, the proposed system can interactively control both micro-mixing and in-situ gelation of hydrogels and thus can be efficiently used in a wide range of biomedical applications.

Acknowledgements

References

[1] H. Suzuki, C.M. Ho, N. Kasagi, J. Microelectromech. S., **13**, 779 (2004).
[2] P.S. Dittrich, M. Jahnz, P. Schwille, ChemBioChem, **6**, 811 (2005).
[3] T.D. Luong, V.N. Phan, N.T. Nguyen, Microfluid. Nanofluid.,**10**, 619 (2011).
[4] A.G. Hadd, D.E. Raymond, J.W. Halliwell, S.C. Jacobson, J.M. Ramsey, Anal. Chem., **69**, 3407 (1997).
[5] E.M. Miller, A.R. Wheeler, Anal. Chem., **80**, 1614 (2008).
[6] G.S. Jeong, S. Chung, C.-B. Kim, S.H. Lee, Analyst, **135**, 460 (2010).
[7] S.J. Kim, F. Wang, M.A. Burns, K. Kurabayashi, Anal. Chem., **81**, 4510 (2009).
[8] S. Mohr, Y. Zhang, A. Macaskill, P. Day, R.W. Barber, N. Goddard, D. Emerson, P. Fielden, Microfluid. Nanofluid.,**3**, 611 (2007).
[9] L.M. Fu, C.H. Lin, Biomed. Microdevices, **9**, 277 (2007).
[10] B.J. Burke, F.E. Regnier, Anal. Chem., **75**, 1786 (2003).
[11] T. Park, S. Lee, G.H. Seong, J. Choo, E.K. Lee, Y.S. Kim, W.H. Ji, S.Y. Hwang, D.G. Gweon, S. Lee, Lab Chip, **5**, 437 (2005).
[12] W.K. Tseng, J.L. Lin, W.C. Sung, S.H. Chen, G.B. Lee, J. Micromech. Microeng.,

16, 539 (2006).

[13] A.C. Apetri, K. Maki, H. Roder, W.K. Surewicz, J. Am. Chem. Soc., **128**, 11673 (2006).

[14] Y.H. Chang, G.B. Lee, F.C. Huang, Y.Y. Chen, J.L. Lin, Biomed. Microdevices, **8**, 215 (2006).

[15] M. Hashimoto, F. Barany, F. Xu, S.A. Soper, Analyst, **132**, 913 (2007).